THE AXOSTYLE OF *SACCINOBACULUS*

II. Motion of the Microtubule Bundle and a Structural Comparison of Straight and Bent Axostyles

J. RICHARD McINTOSH

From the Department of Molecular, Cellular, and Developmental Biology, University of Colorado, Boulder, Colorado 80302

ABSTRACT

Undulations of the flagellate *Saccinobaculus* result from motility in its axostyle, a bundle consisting of thousands of cross-bridged microtubules. In its resting state, the axostyle is a helix of large pitch and slowly varying radius. The active state as seen by light microscopy involves first a bending of the anterior end of the axostyle to a radius of about 8 μm with a circular arc ranging from 60° to 180°, and then the propagation of this bend without damping to the posterior end of the organism at speeds up to 100 μm/s. The cross section of an unbent axostyle is crescent shaped. This crescent flattens as the bend arrives and reappears as the bend passes by. Intertubule bridges impart to the axostyle tubules an axial periodicity of about 150 Å which can serve as a marker for the investigation of tubule sliding or contraction associated with bend formation. Optical diffraction measurements on electron micrographs of the bend demonstrate that the axostyle tubules slide over one another and that the tubules on the inside of a bend usually contract, sometimes by as much as 25%. Possible relationships between the contraction and sliding of the tubules are discussed.

INTRODUCTION

The axostyle of *Saccinobaculus* is an intracellular bundle of several thousand cross-bridged microtubules about 100 μm long that propagates a wave of bending from its anterior to its posterior end (Grimstone and Cleveland, 1965). In another study of axostyle structure we show that the microtubule bundle displays almost crystalline regularity, with an average unit cell consisting of four approximately parallel segments of microtubule about 150 Å long and the bridges between them (McIntosh et al., 1973). In this paper we describe changes which occur in the unit cell when the axostyle bends. Possible relations between these structural changes and the mechanism of microtubule motile activity are discussed.

MATERIALS AND METHODS

Specimens were collected and prepared for light and electron microscopy as previously described (McIntosh et al., 1973). Movies of actively swimming cells were prepared with Zeiss Zernike phase-contrast optics and a 16 mm camera at speeds of about 32 frames/s. Electron micrographs were taken on a Philips 300 electron microscope equipped with a goniometer stage permitting 45° of tilt in any direction.

Measurements were made on plates with a Nikon Shadowgraph 6C. Optical transforms of electron micrographs (Klug and Berger, 1964) were prepared with a diffractometer modified slightly from the design of Klug and DeRosier (personal communication): a Spectra-Physics model 120 5 mW He-Ne

laser (Spectra-Physics, Mountain View, Calif.) fitted with a beam-expanding telescope was used to form a 1 inch-wide beam of slightly converging light. The diffraction pattern was viewed with a lens-less Nikon camera equipped with a reflex light meter and rotatable Polaroid filter for intensity control. The laser and a front-surfaced mirror are placed on a 2 m optical bench and the camera is on a 0.5 m bench, near enough to the specimen so that the operator can manipulate the electron micrograph and a mask which delimits the field of view while watching its diffraction pattern. A real image of the diffraction specimen can be recorded with the camera by placing a convex lens at the correct place on the bench. A red filter on the camera allows operation in room light.

The absolute accuracy of our measurements is probably no better than ±8%, but the regularity of the axostyle permits comparisons at far higher precision. The values for intertubule spacing and paraxial period presented in the previous paper (McIntosh et al., 1973) were taken as correct, and the axostyle itself was then used as an internal standard. Measurements of periodicity changes using the diffractometer to compare different portions of a single plate are probably good to ±2%.

OBSERVATIONS

Shape of the Axostyle Bend and a Description of Bend Propagation

Figs. 1 *a* and *b* show that the axostyle bend is a circular arc to an excellent approximation. The dark circular line outside each bend was drawn with a compass. At higher magnification one can trace a single tubule with a compass over as much as 90° of arc. It is also evident from Fig. 1 that the arc length of the bend varies markedly from cell to cell. Frame-by-frame analysis of movies has shown, however, that in a given cell, the radius of bend curvature (Rb) and the extent of the arc are approximately constant as the bend propagates (Fig. 2).

The velocity of bend propagation shows tremendous variation and seems to be a sensitive assay for the health of the cell. The fastest propagation recorded was over 100 μm/s. In cells which are about to cease beating, the bend will almost stop moving partway down the axostyle and then speed up again, radius and arc length constant the while. The region of low velocity in such cells can

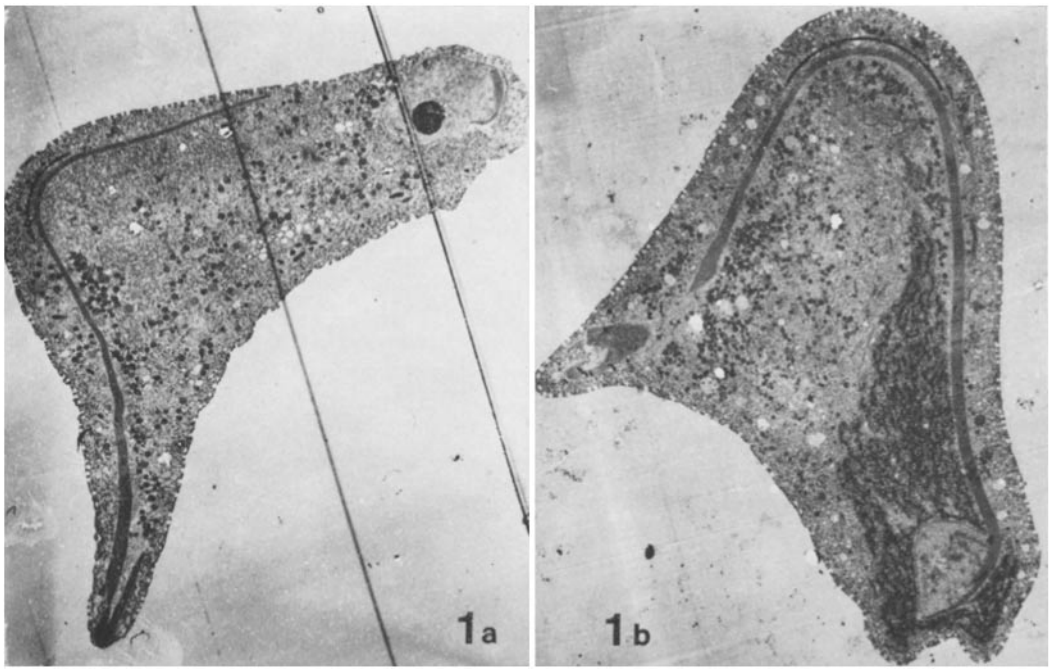

FIGURE 1 Two S.l cells showing the circular arc of the bend, and the variation in total bend arc. The dark circular line outside each bend was drawn with a compass. × 1000.

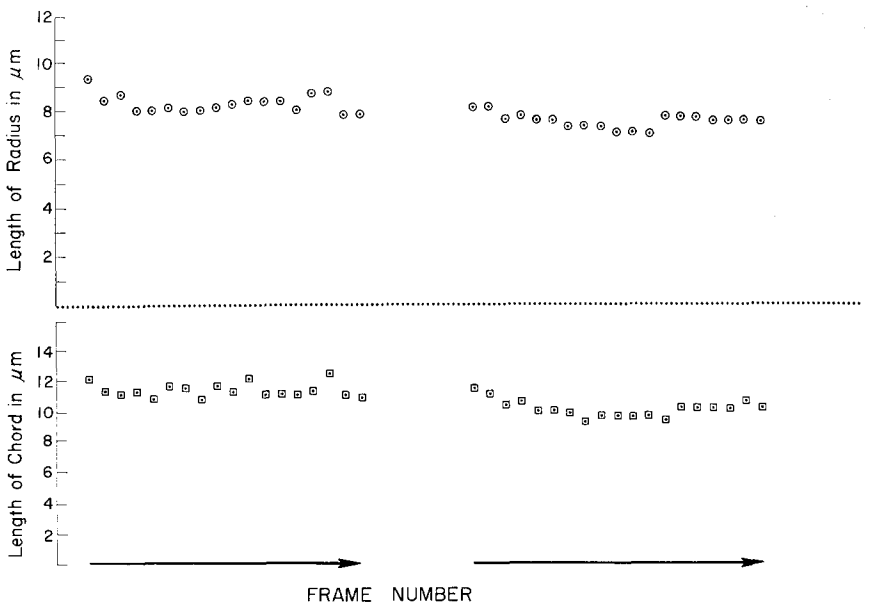

FIGURE 2 Measurements of bend radius and of the longest bend chord as a function of movie frame number for the propagation of a single wave from two specimens of S.a. Data were collected from prints similar to those shown in Fig. 3. The framing rate was 32 frames/s.

vary randomly from one wave to the next (an interval of 1–10 s), indicating that the velocity variation is not simply a result of major changes in the physical properties of the cytoplasm. It follows from the constancy of bend curvature (no damping) and from the ability of the wave to speed up in transit that the propagation is not a passive phenomenon; chemical energy is probably converted to mechanical work as the bend travels.

Our movies of bend propagation in healthy, fast-swimming cells have revealed a difference from previous reports on the nature of bend motion (Cleveland et al., 1934; Grimstone and Cleveland, 1965). As the bend travels the length of the axostyle, the plane of the bend rotates about the long axis of the cell by an amount equal to the total twist in the axostyle helix before the bend is formed, less any rotation of the cell itself. Further, the axostyle is redirected as the bend passes by an amount equal to the arc subtended by the bend, less the amount of redirection in the portion of the axostyle posterior to the bend (Figs. 3 *a–j*). We conclude that the apparently complex motion of *Saccinobaculus* may be interpreted simply as the result of a circular arc propagating down a helical ribbon (Fig. 4). The cell itself reorients and rotates as the bend moves, as if the ends of the motile ribbon were firmly attached to the cell cortex. Figs. 3 *a-j* also show that a second bend may start down the axostyle before the first has run off the posterior tip, and that the nuclear side of the axostyle is the inside of successive bends.

Electron micrographs of serial cross sections from two cells fixed with the bend in transit show that the left-handed sense of the axostyle helix (we have determined axostyle helix sense in six cells) does not change at the bend. Since the bend always moves from anterior to posterior, it follows that the organism is continually rotated in one direction by successive bends.

A Comparison of Structure in Straight and Bent Regions of the Axostyle

There are two large species of *Saccinobaculus*, *Saccinobaculus lata* (S.l) and *Saccinobaculus amblo-axostylus* (S.a) (Cleveland, 1950). When the S.l axostyle bends, the crescent seen in cross section flattens (Figs. 5 *a* and *b*). In S.a the flattening is sometimes incomplete. For example, in one bend of an S.a axostyle the minimum radius from the center of crescent curvature to the outermost row of the axostyle (R_c^o min) increased from 7 μm ± 10% posterior to the bend to about 9 μm ± 8% in the bend (Fig. 6 *a*), a change of just over 2 SE.

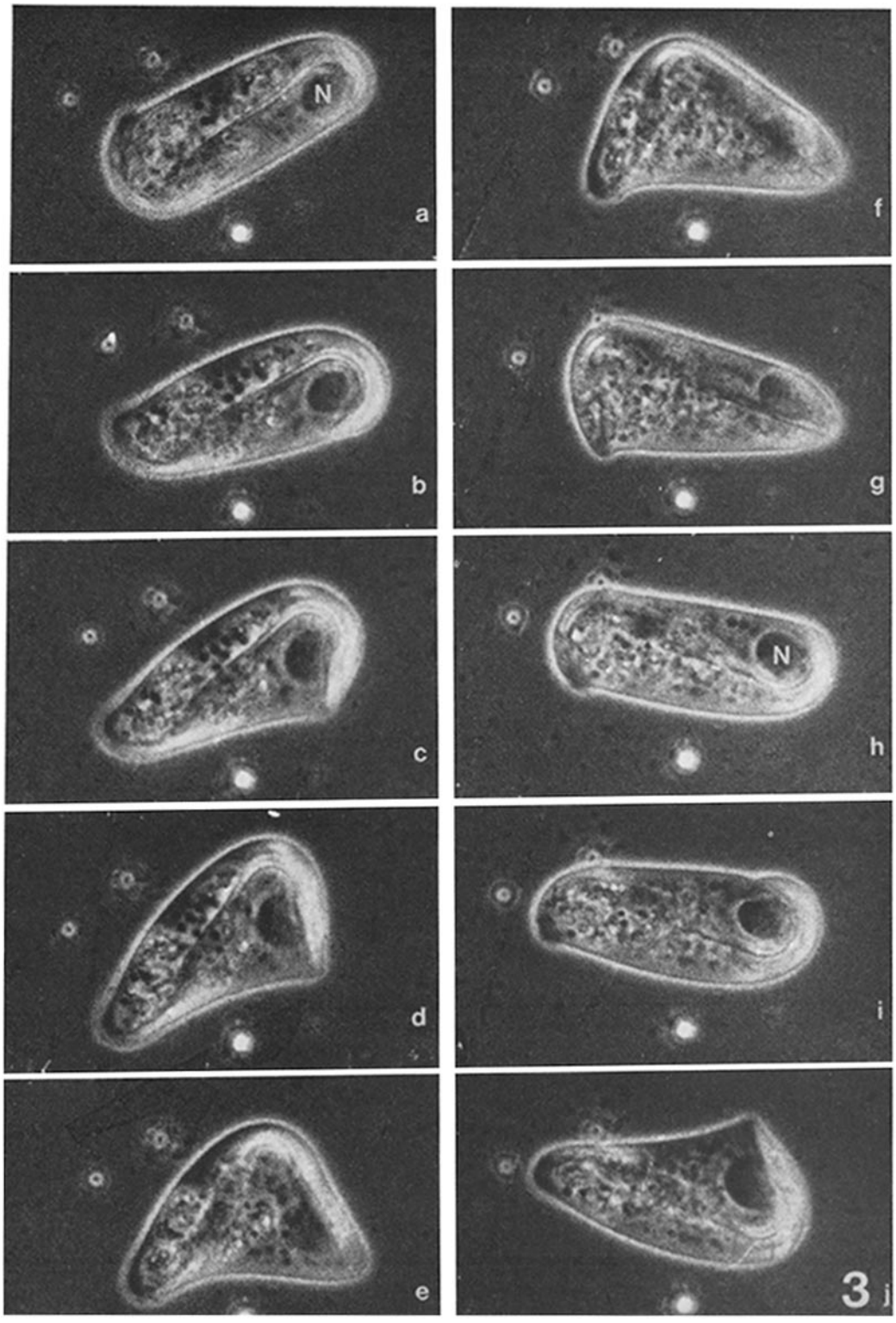

FIGURE 3 A print-out of frames spaced about 100 ms apart, from a phase-contrast movie of a swimming S.a cell. *N* marks the nucleus. The sequence shows that the arc of the bend defines the reorientation of the axostyle, and that the bend is approximately constant as it propagates. × 450.

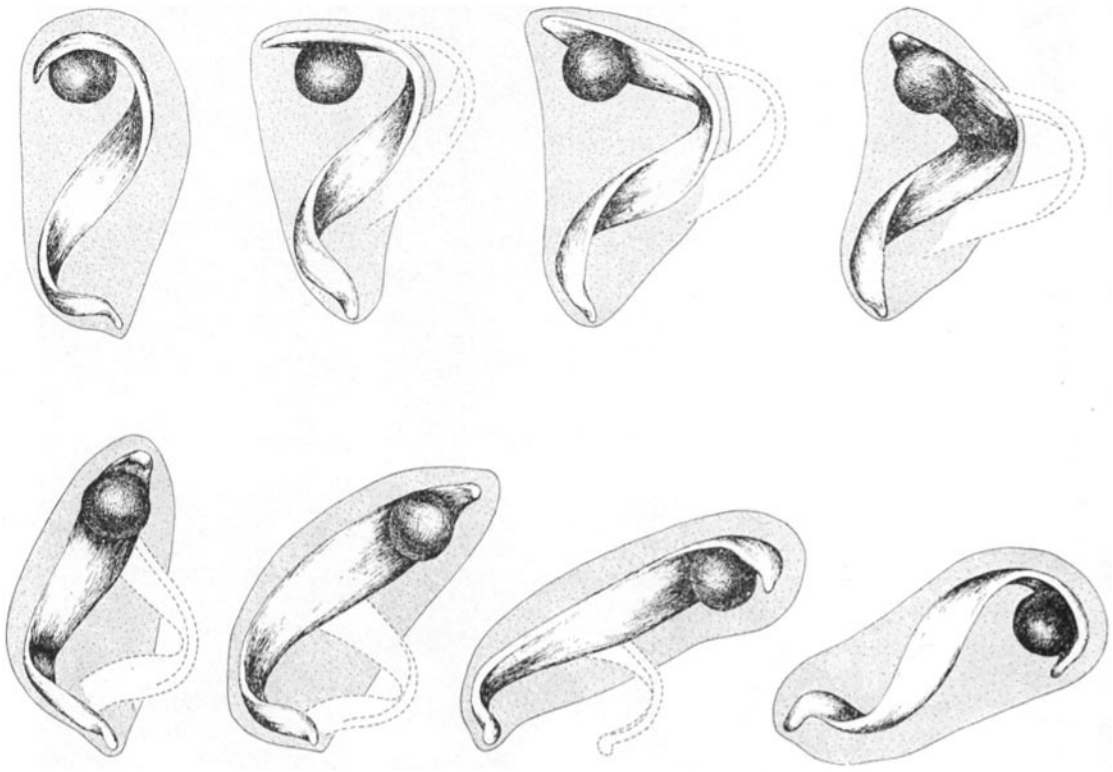

FIGURE 4 An artist's reconstruction of the propagating bend. The axostyle action is portrayed as a circular arc, propagating down a helical ribbon. For clarity, no redirection of the axostyle posterior to the bend is shown. The dotted lines show what the bend would look like if the observer walked around the cell as it rotated.

(For a discussion of crescent curvature, see McIntosh et al., 1973.) Fig. 6 *b*, on the other hand, shows a second bend near the nucleus in the same cell, and here the crescent is essentially gone. The crescent re-forms in both species after the bend passes by.

We have compared the population of interrow bridges in the bend with the population of these bridges in straight portions of the axostyle. In S.l, there are 0.46 times as many interrow bridges as intrarow links in a straight region of the axostyle (n = 3760), but there are only 0.29 times as many interrow bridges as intrarow links in a bent region (n = 4400). In S.a there is no significant difference in this fraction from straight to bent regions: 0.19 vs. 0.20 (n = 3960 in each case).

Longitudinal sections of the bend are theoretically more informative about the bending mechanism than are cross sections. When a bundle of fibers bends, there are only two independent axial strains which will allow the bundle to accept the new shape: fiber length may change, so that the fibers on the inside of the curve become shorter than the fibers on the outside, or fiber length may remain unchanged while fiber position is altered (Figs. 7 and 8). We call these the contracting and the sliding models for bend formation. Any linear combination of the two models is also possible. The tubules of both S.l and S.a show an axial periodicity due to the projection of intertubule links onto the tubules' surfaces (McIntosh et al., 1973). Measurement of axial tubule periodicity as a function of position on the radius (Rb) from the center of bend curvature (CB) should allow one to determine the relative contributions of the two strains to bend formation in the axostyle. Thus, if the axostyle tubules contract, a scan moving outward along any given radius of the bend should reveal variation in axial periodicity (See Figs. 7 and 8).

The magnitude of the strain necessary to form a given radius of bend increases with the thickness of

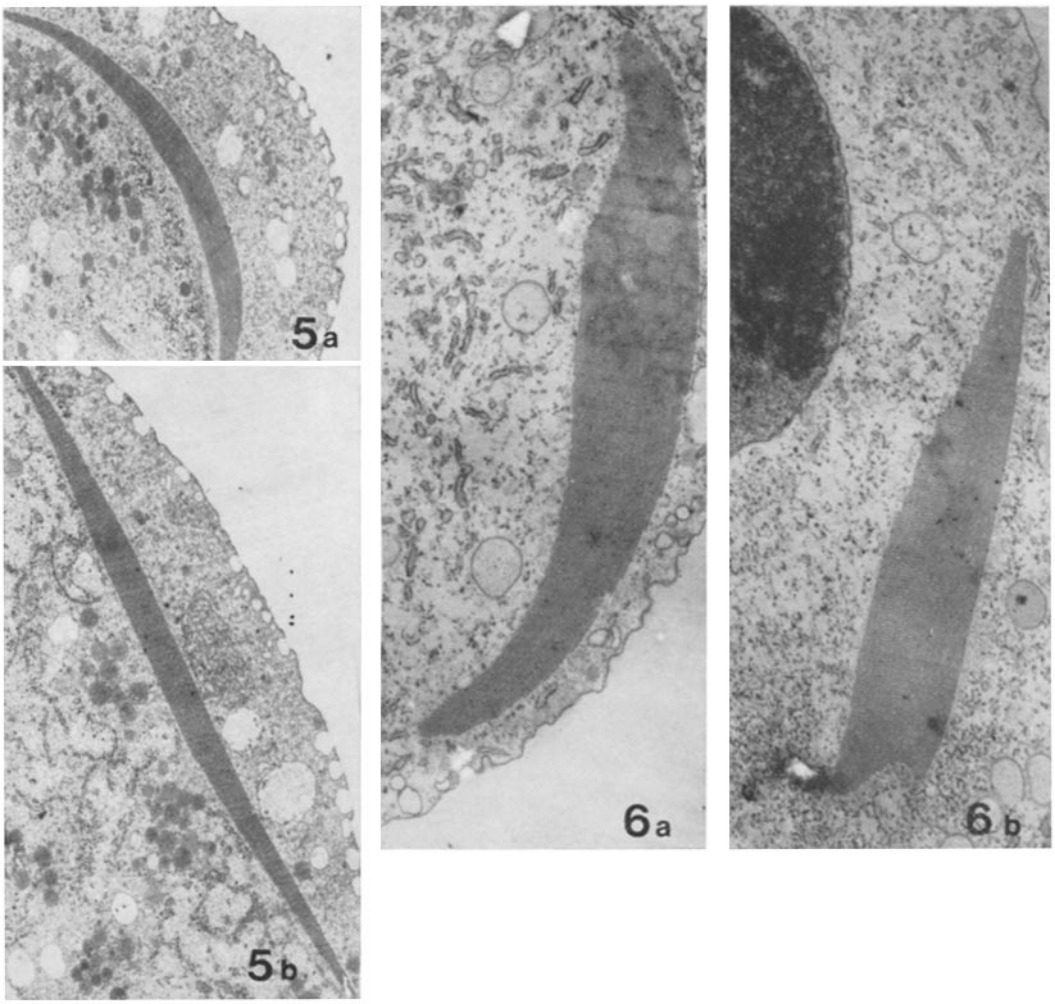

FIGURE 5 Cross sections of an S.l axostyle. Fig. 5 *a* is from an unbent region of the axostyle posterior to the bend. The section is tilted by 45° to bring the tubules into good cross section. Fig. 5 *b* is from the middle of the bend in the same cell. The section is untilted. × 4600.

FIGURE 6 Cross sections showing crescent curvature in bent regions of an S.a axostyle. Fig. 6 *a* is from a bend near the posterior end of an organism. Fig. 6 *b* is from a bend near the nucleus in the same cell. × 11, 000.

the axostyle along the bend radius (Fig. 7). The S.a axostyle contains as many as 66 tubule rows, while S.l has only about 25 rows, so most of our work on bend structure has been done with S.a. Further, the periodic arms seen in longitudinal section of the S.a tubules increase the intensity of the intrarow link periodicity, adding to the attractiveness of S.a as a specimen for study.

Straight regions of the S.a axostyle show clear optical diffraction patterns (transforms) (Figs. 9 *a* and *b*). The two orders of a 340 Å equatorial spacing correspond closely to the interrow distance measured on micrographs (three cells). Often a third and fourth order are seen on the equator. (In Table I there are six drawings of transforms along with explanatory text to help in the viewing of the patterns presented here.) There is occasionally (two cells) an equatorial spot at 265 Å which will not index with the others. The significance of the extra spot is not yet clear, but

the equatorial spacings might be the third and fourth orders of the reflection from a four-tubule cluster which is often seen. There is a 150 Å layer line which we attribute to reflection from the intrarow links and tubule arms, the "dog-ears" described in the previous paper (McIntosh et al., 1973). A layer line is clearly visible in selected images of S.1 as well (Fig. 9 *c*). The angle between the reciprocal lattice vectors is variable from

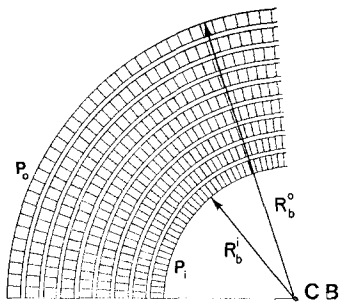

FIGURE 7 A longitudinal representation of the contractile model for bend formation. The periodicity on the inner edge of the curve (P_i) is less than the periodicity on the outer edge (P_o). R_b^i is the radius from the center of the bend (CB) to the innermost tubule row; R_b^o is the radius to the outermost row. For pure traction, $(P_o)/(P_i) = (R_b^o)/(R_b^i)$.

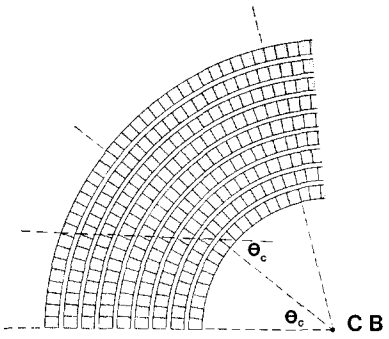

FIGURE 8 A longitudinal representation of the sliding model for bend formation: $P_o = P_i$. In this model lines joining equivalent points on adjacent tubules remain approximately parallel to the radius at the onset of curvature for angles less than about 45°. Note that there is some critical angle, θ_c, at which the radius from CB to the n^{th} periodicity on the outermost tubule passes through the $(n\text{-}1)^{th}$ periodicity on the first tubule in, the $(n\text{-}2)^{th}$ periodicity on the second tubule in, and so forth. θ_c is a long-range periodicity around the curve, because the local relationships along each radius making an integral multiple of θ_c with the radius at the onset of curvature are indistinguishable from each other.

micrograph to micrograph in both species. We nterpret the angle as the diffraction analogue of the shifting registration lines (imaginary lines connecting neighboring intrarow links on adjacent tubules which can be seen by viewing micrographs such as Fig. 27 *a* of McIntosh et al., 1973, from the side). When the registration line is perpendicular to the tubule axis, there is a diffraction spot on the meridian and the reciprocal unit cell is a rectangle.

We have masked longitudinal sections of axostyle down to two and then to one microtubule. The essential features of the layer line seen in Figs. 9 *a* and *c* are preserved with two tubules (Figs. 10 *a* and *b*), but with only one tubule there is a single major layer line reflection just off the meridian (Figs. 10 *c* and *d*). We attribute the off-meridian placement of the major layer line spot to a slightly oblique orientation of the intrarow links relative to the plane perpendicular to the tubule axis.

Optical transforms can be used to look for axostyle lattice changes as the bend forms. Figs. 11 *a–f* show an illustrative series of transforms prepared from the contractile model for bend formation (Fig. 7), and Figs. 12 *a–h* are the same for the sliding model (Fig. 8). Only the first few diffraction orders are shown in order to keep the transforms similar to those from electron micrographs. The arcing of the equatorial reflections is due to the exaggerated curvature of the pictorial tubules which was included to clarify the structural implications of each model. The distance from the layer lines to the equator is a measure of the reciprocal of the periodicity along the tubules. In the contractile model, the layer line is smeared from the diversity of paraxial periods (Figs. 11 *a* and *b*), and the intensity maximum of the smear moves out as one scans in along the bend radius (Rb) (Figs. 11 *c–f*).

In the sliding model the layer line is not smeared (Figs. 12 *a* and *b*), and the position of the layer line does not vary with a scan along Rb (Figs. 12 *c–f*). With a scan around the bend arc, the orientation of the equator changes relative to the spots on the layer line (Figs. 12 *c–f*). The angle between the lattice vectors of the reciprocal unit cell changes to match the changes in the real unit cell (Fig. 8). Since all the paraxial periodicity lines have been drawn on bend radii, the portion of the layer line which is clearly seen tends to shift with the equator, but for small shift angles the change in the angle between the reciprocal lattice

vectors is equal to the arc swept out at the bend center. At some angle θ_c, where $\tan \theta_c = P/\Delta Rb$ (P is the axial periodicity and ΔRb is the center-to-center spacing of the rows), the pattern repeats at a new orientation (Figs. 8 and 12 *g* and *h*).

Fig. 13 is the transform of a straight portion of the S.a axostyle posterior to the bend, just above the area shown in Fig. 14. The 150 Å layer line is evident. Fig. 15 is the transform of the region marked *O* on Fig. 14 at the outer edge of the curve. The distance from the layer line to the equator is unambiguous, even though the spots on the layer line are not distinct. P_o is about 142 Å. This small change from the periodicity in the straight region may result from orientation artifact. (The helical arrangement of the axostyle tubules gives them a changing orientation with respect to any one plane of section.) Fig. 16 is the transform of the region marked *M* on Fig. 14. The 142 Å layer line shown in Fig. 15 is still present, and a new layer line has appeared at 126 Å. Fig. 17 is the transform of the region marked *I* on Fig. 14. The 142 Å line is now gone, the 126 Å line remains, and a new one has appeared at 105 Å.

These data show that the tubules of this S.a axostyle display three different axial periodicities when the axostyle is bent. The population of intermediates between the periodicities is not above noise level. The results were reproducible in two cells, but two other S.a cells have shown only two length states: one at about 140 Å on the outside of the bend, and one at about 125 Å on the inside. The number of states seems to be related to the number of tubule rows contained in the sections under observation.

Since the tubules of different rows are tilted relative to one another (McIntosh et al., 1973), the tubules at different bend radii necessarily make different angles with the plane of section. This orientation variation will give rise to different values for the tubule periodicities as seen projected onto a photographic plate. Some variation of observed tubule periodicity with Rb is therefore expected, even without any tubule shortening. We have excluded the possibility that orientation effects account for our observations of tubule shortening on the inside of a bend by choosing a plane of section which makes a greater angle with the tubules at the outside of the bend than with those on the inside. Thus the orientation artifact will reduce the observed tubule shortening, not increase it.

We have looked for changes in axostyle tubule diameter associated with bend formation but have found none. Since the simple assumption of a constant tubule volume suggests a diameter change of less than or equal to 5%, it is not surprising that direct measurements with a microcomparator have failed to reveal a cross-section difference between straight and bent tubules.

Although the existence of discrete tubule periodicities excludes the possibility of uniform contraction as a sufficient explanation of bend formation, we can ask whether the observed contraction is quantitatively sufficient to account for bend curvature (Fig. 18). The ratio of the inside axial periodicity (P_i) to the outside axial periodicity (P_o) is 0.74 for the bend shown in Fig. 14. This is approximately equal to the ratio of the corresponding radii of curvature: $(R_t^i)/(R_b^o) = 0.76$ as measured with a compass on prints. It follows that tubule contraction, as seen by decrease in bridge-binding periodicity, is sufficient to account for bend formation in this cell. If an accurate correction for orientation artifact were possible, the contraction might exceed the amount necessary for bend formation.

The transforms of areas like *M* in Fig. 14 show that groups containing as many as 25 tubule rows behave as constant periodicity units (CPU) (Fig. 18). The lack of contraction within a CPU demands that the tubules of the unit slide relative to one another to allow smooth bend formation. To check this deduction we have prepared diffraction patterns from small regions within a CPU and scanned along the bent tubules. For S.a, $\theta_c = 24°$ using the largest periodicity and radius seen, so $\pm 12°$ is the largest possible variation in the angle between reciprocal lattice vectors. Fig. 19 is a series of transforms from the CPU in the middle of Fig. 14. The reflections from the mask edges serve as markers of constant orientation, and the specimen was shifted so that for pure sliding behavior the bridge reflections would not move while the equator rotated. Figs. 19 *a* and *b* show pure sliding over an arc of about 8°, but with further shifting (Fig. 19 *c*) new layer line spots appear, just as in the sliding model (Fig. 12). We tentatively attribute the new spots both to a shift in the position of the intense region of the layer line due to radial orientation of successive bridges and arms (as in the transform of the sliding model), and to a sampling of different tubules due to the obliqueness of the section relative to the tubules'

axes. Thus, the fit to a pure sliding model within a CPU is good over limited arcs.

We have examined the onset of curvature in S.a. Figs. 20 *a–c* show transforms from a straight region and from the zone in which the bend is forming in the same section shown in Fig. 14. The transform of the forming curve shows a change of the 150 Å layer line (Fig. 20 *a*) into a smear, running from 145 Å to 135 Å (Fig. 20 *b*). When the bend is almost formed, two discrete states are seen: 142 Å and 130 Å (Fig. 20 *c*). Further contraction occurs to give the pattern seen in Fig. 16. Apparently we are seeing the development of the axostyle strains as we track along the axostyle from the posterior to the anterior portions of the bend, but further work is needed to clarify the details of the process.

Since the S.l axostyle is about the thickness of a single CPU in S.a, we have also examined bends in this species for contraction and sliding. In S.l we have observed no discrete contraction in three cells. In this species P_o is 130 Å, slightly but significantly less than the axial period in straight portions of the axostyle (140 Å). P_i is generally less than P_o (See Figs. 21 and 22 *a–e* and their legends). To assess whether the observed contraction is sufficient to account for the bend, we have defined a parameter,

$$Z = \frac{(P_o - P_i)\ \text{observed}}{(P_o - P_i)\ \text{theoretical}},$$

where $(P_o - P_i)$ theoretical is given by $P_o\frac{R_o - R_i}{R_o}$ as expected in pure contraction. The values of Z calculated for different places from individual sections of S.l axostyles are given in Table II along with the number of rows where the observation was made. Z varies from 0.00 to 0.59, with a mean value of $0.167 \pm 101\%$; it never approaches the 1.00 predicted from a pure contracting model. A scan along the bend arc in S.l again provides direct but limited evidence for sliding of the tubule rows during bend formation (Figs. 22 *f–i*).

Discussion of Axostyle Action

Since a circle is an arc of constant curvature, the circularity of the axostyle bend implies that the bending mechanism can function without complex time-dependent variations. Further, the constancy of both bend radius and bend arc length during propagation implies that there are no long-range variations of the bending mechanism with either time or space: analysis of the bend at one location should serve for all locations, and away from the

FIGURE 9 Fig. 9 *a* is the diffraction pattern (transform) of the field of the straight S.a axostyle shown in Fig. 9 *b*. Fig. 9 *c* is a similar pattern for S.l, letting the edge of the laser's circular beam define the area viewed. Three equatorial orders are clear, but there is only one layer line.

FIGURE 10 Figs. 10 *a* and *b* show diffraction from two tubules in the field of Fig. 27 *a* of McIntosh et al. (1972). A print is used for Fig. 10 *a* because the tubule image seen with the laser through the image-forming lens was obscured by out-of-focus diffraction from the knife edges of the mask. Figs. 10 *c* and *d* correspond to Figs. 10 *a* and *b*, but for a single tubule.

FIGURE 11 Diffraction from the contraction model (Fig. 7). Fig. 11 *b* is the transform of Fig. 11 *a*, *d* of *c*, and *f* of *e*. Note that the layer line is smeared in Fig. 11 *b* where many paraxial periodicities are seen. Moving from the outside of the bend (Figs. 11 *c* and *d*) to the inside of the bend (Figs. 11 *e* and *f*) we see an outward motion of the layer line (the reciprocal relationship between periodicities in real space and in diffraction space).

FIGURE 12 Diffraction from the sliding model (Fig. 8). Fig. 12 *b* is the transform of Fig. 12 *a*, *d* of *c*, *f* of *e*, and *h* of *g*. The layer line is not smeared in Fig. 12 *b* because only one paraxial period is present. Moving from outside to inside of the bend does not cause the layer line to move away from the equator (Figs. 12 *c* and *d* compared with Figs. 12 *e* and *f*), while a small shift around the arc of the bend causes a rotation about the central maximum of the region of high spot intensity. During this shift, the layer line spots themselves do not move, so there is a concomitant change in the angle between the spots on the layer line and the equatorial reflections from the tubules (Figs. 12 *c–f*). Further shifting, as in Figs. 12 *g* and *h*, reveals the repeat in the pattern when θ_c is reached.

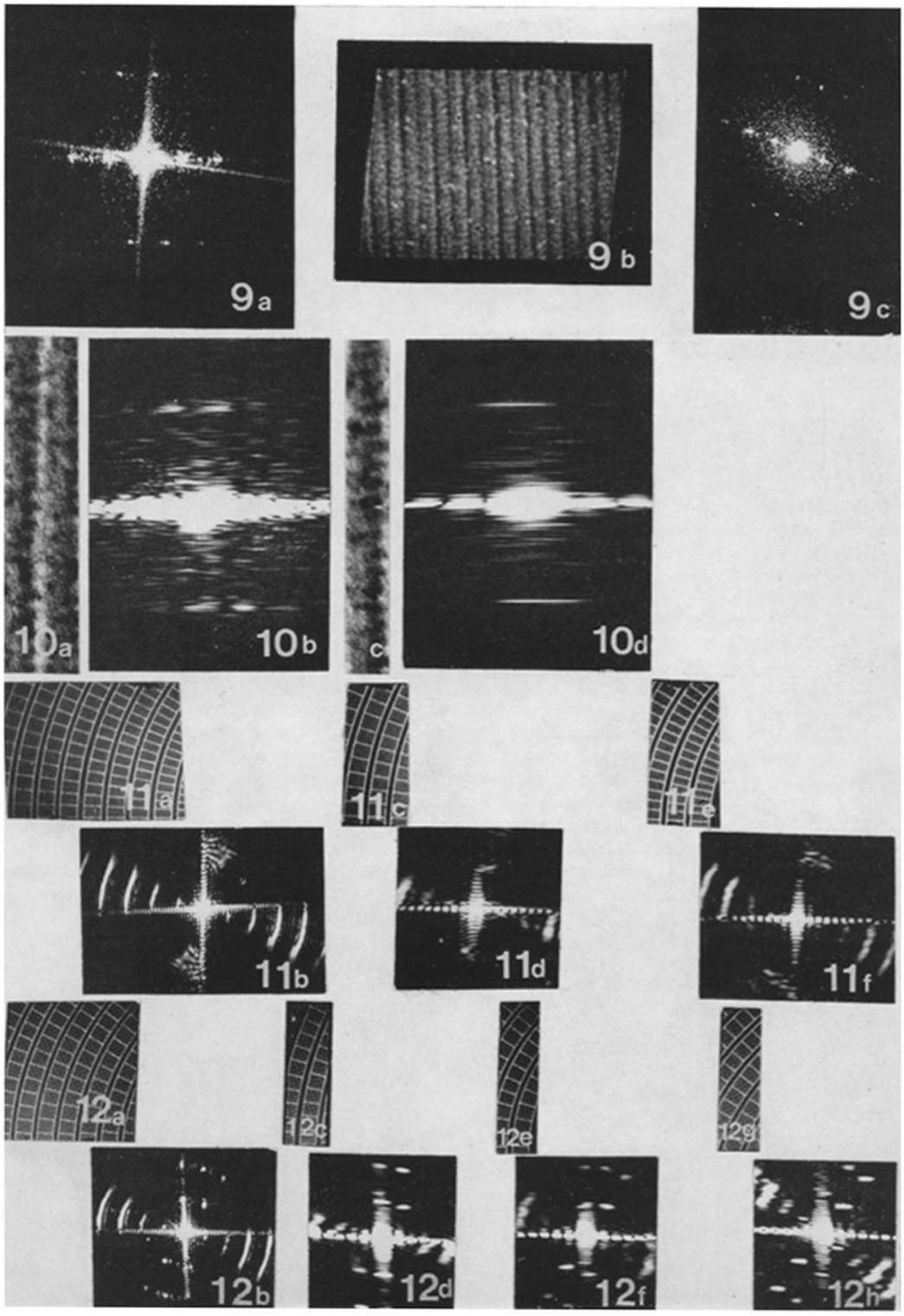
9a
9b
9c
10a
10b
c
10d
11c
11b
11d
11f
12a
12c
12e
12g
12b
12d
12f
12h

TABLE I

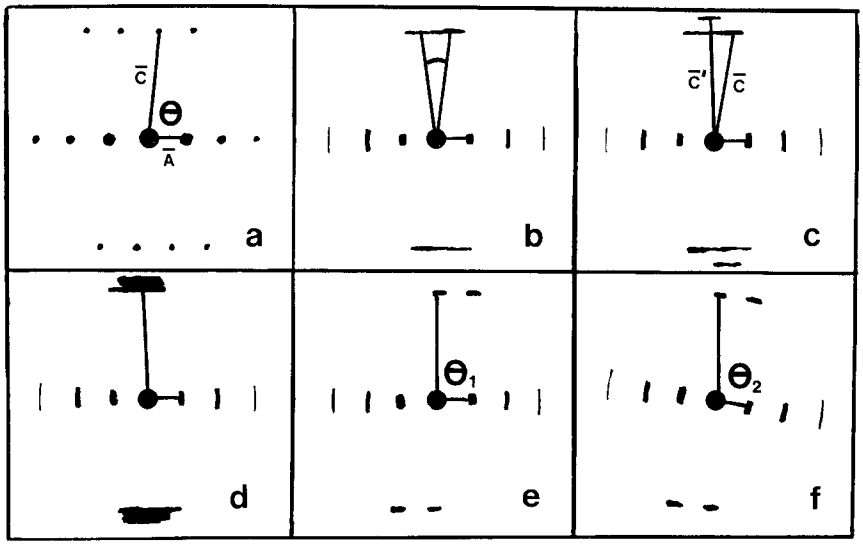

(*a*) *Straight axostyle.* There are three horizontal rows of spots. The middle is called the equator, the other two are layer lines. The biggest spot on the equator (brightest) is the central maximum. The lines labeled $\bar{A}$ and $\bar{C}$ interconnect neighboring points in such a way as to define a lattice for all the points shown. On a diffraction pattern this is called the "reciprocal lattice" and arrows connecting the central maximum with neighboring points are called "reciprocal lattice vectors." The angle θ is the angle between $\bar{A}$ and $\bar{C}$. Diffraction spots along the equator come from a horizontal periodicity, e.g., evenly spaced microtubules running vertically. The layer lines come from a vertical periodicity, e.g., periodic projections from the surfaces of the vertical microtubules. The angle θ depends upon the registration of the periodic projections on adjacent tubules. (*b*) *Bent axostyle.* In an axostyle bend, the spots on the equator will arc as shown. The extent of arc will depend upon the amount of arc on the bend which is illuminated by the laser beam when the diffraction pattern is made. The spots on the layer line arc too, but their arcing is within the layer line, tending to make them fuse. The layer line spots will also fuse if the periodic projections from adjacent tubules fall out of register. (*c*) *Bent axostyle with discrete axial contraction.* If there are two discrete layer lines close together, as shown ($\bar{C}$ and $\bar{C}'$), there are two axial periodicities in the region of the bend under examination. (*d*) *Bent axostyle with simple contraction.* If the layer line is thick, there are many axial periodicities present. This would correspond to a contracting tubule situation. (*e* and *f*) *Bent axostyle with sliding of adjacent tubules.* In well-oriented regions of the axostyle, diffraction from a small portion of a bend will show discrete spots on the layer line. The angle θ can be measured with considerable precision. Θ can be used to determine tubule sliding because in a pure sliding situation θ will vary as a function of the position of the laser spot on the bend arc. With a scan around the bend of 8° of arc, θ should change by 8°.

axostyle extremes, different bends should be comparable without correction for position. The lattice-like structure of the axostyle (Grimstone and Cleveland, 1965; McIntosh et al., 1973) indicates that whatever the cause of bend formation, it is a transition occurring in the unit cell consisting of about 150 Å of axial length in four neighboring tubules and the bridges between them.

The bend-dependent flattening of the cross-section crescent may be interpreted as a passive strain which serves to minimize the potential energy stored in the bend, like the flattening of the cross section of a carpenter's tape measure as it is bent. It is possible, however, that active mechano-chemical transductions are coupled directly to the flattening and re-formation of the crescent. Since the axostyle rigidity is dependent upon the curvature of the tubule rows, local crescent flattening could be used to produce weak zones in the axostyle. One possible model for axostyle bend formation is based on the postulate that some external force, such as the surface tension in the

cell membrane, bends the axostyle where it has been weakened by crescent flattening. A propagating return of row curvature would cause the bend to travel.

We dismiss this model for bend formation as unlikely for two reasons. In some cells, the axostyle bend contains as much as 180° of arc (Fig. 1 *b*); the cell membrane and cortex are deformed from following the shortest path from one end of the axostyle to the other. Further, the morphology of the anterior end of the cell renders doubtful a mechanism dependent upon the transmission of compression from the cell surface to the anterior end of the axostyle (McIntosh et al., 1973). We therefore consider it improbable that bend formation results from forces external to the axostyle, though we cannot exclude the possibility of an active process directly coupled to crescent flattening.

When tubule sliding and tubule contraction coexist, as in all cases of S.a and in some views of S.l, one can postulate that either or both strains are causal in bend formation. Since, however, some views of S.l are found which show sliding with no measurable shortening of the tubules on the inside of the bend relative to those on the outside, we may deduce the sufficiency of sliding in those cases of bend formation. It is therefore possible that sliding is the only strain which is directly coupled to mechanochemical transduction, and that contraction and crescent flattening are really a yielding of the axostyle structure to stress generated by the sliding mechanism. Some sort of contraction necessarily accompanies a sliding model of axostyle bending for the following reason. Pure sliding involves the introduction of lattice dislocations, and since the bend always forms with the nucleus on the concave side and propagates toward the tail, all the dislocations are of the same sign. Their reiteration would rapidly destroy the axostyle. We suggest that the observed tubule shortening accompanies sliding and prevents axostyle destruction by gradually "absorbing" the dislocations introduced by sliding. Consistent with this view is the occasional observation of a variation in tubule periodicity in a straight region of the axostyle immediately after the bend, as if not all the tubule sheer had been removed within the bend itself.

The process of tubule contraction is interesting in its own right, even if it is not the active process in bend formation. Summers and Gibbons (1971) mention the possibility that similar processes occur in flagellar beating. We think that fixation artifact is an implausible explanation for tubule shortening, given the general reliability of the aldehyde fixatives, the similarity of living and fixed cells as seen in the light microscope, and the constant curvature of the axostyle bend throughout the electron microscope preparation procedures. Fitzharris et al. (1972) have shown that the arc length and radius of the bend in *Pyrsonympha* axostyle do not vary as the velocity of bend propagation drops to zero within 2 s after addition of the same fixative used here. Recent structure studies have shown that microtubules can exist with at least two surface lattices. Cohen et al. (1971) have described a dehydration-dependent transition in the surface lattice of isolated sperm tail microtubules as seen with X-ray diffraction. Thomas (1970) has also seen variation in the structure of microtubules. The changes in *Saccinobaculus* tubule periodicity may involve analogous transitions, but apparently the several tubule periodicities of the axostyle bend can all exist under physiological conditions.

The significance and universality of microtubule contraction are at this time open to question, given our evidence that sliding is a sufficient mechanism for bend formation, and the evidence for the importance of sliding in other microtubule-containing motile systems (Satir, 1965; McIntosh and Porter, 1967; Bannister and Tatchell, 1968; Huang, 1970; McIntosh and Landis, 1971; Summers and Gibbons, 1971). The most useful aspect of axostyle bend formation may ultimately be the zone in which the bend is forming, where pictures of S.a show intermediate contracted states. Further study of this zone may reveal the morphological features of the bending mechanisms and provide clues on causal relationships between tubule sliding and contraction.

The author thanks Edward Ogata for making the movies of *Saccinobaculus* and Ruth Sharp for her careful measurements on them. The technical assistance of Kenneth Vanderslice, Story Landis, and Cathy Gelpke was invaluable. I thank Doctors D. Caspar, J. Pickett-Heaps, and G. Borisy for their reading of an earlier version of this manuscript.

This work was supported in part by a Biomedical Research grant and a Health Sciences Achievement Award to the University of Colorado, and by GB-25876 from the National Science Foundation and American Cancer Society Grant VC-9 to J. R. McIntosh.

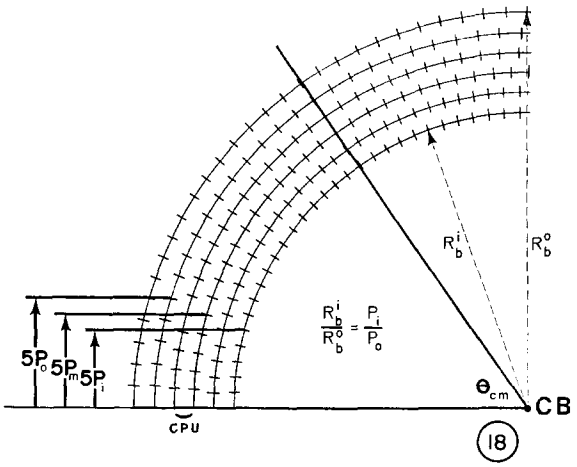

FIGURE 13 Transform of a straight portion of the axostyle shown in Fig. 14, the area posterior to the bend and just above the top of the picture seen here. The layer line is at 150 Å.

FIGURE 14 A bend in an S.a axostyle tilted 35° from horizontal. The dark precipitate is stain artifact. Transforms of the areas marked *O*, *M*, and *I*, are shown in Figs. 15, 16, and 17. × 22,000.

FIGURE 15 Transform of the region marked *O* on Fig. 14. The layer line is at 142 Å. The off-meridian spots in the first and third quadrants near the equator can be accounted for by section artifact since the malorientation of the tubules causes them to enter and leave the section at a periodicity of about 1000 Å. There are similar artifactual spots in Figs. 16 and 19.

FIGURE 16 Transform of the region marked *M* on Fig. 14. Two layer lines are now seen, one at 142 Å, the other at 126 Å. The diffracted intensity between them is not above noise level. The inner layer corresponds to the single line in Fig. 16.

FIGURE 17 Transform of the region marked *I* on Fig. 14. The inner layer line corresponds to the outer layer line in Fig. 16; the outer represents a new paraxial periodicity of 105 Å.

FIGURE 18 A diagram showing bent fibers (lines) possessing three discrete axial periodicities, and thereby depicting three constant periodicity units (CPU). The contraction is quantitatively sufficient for bend formation, but sliding must occur within each CPU. θ_{cm} is the critical angle for $P_m \cdot \theta_{ci}$ corresponding to P_i (unmarked) is slightly less, and θ_{co} for P_o (unmarked) is slightly more.

FIGURE 19 A series of transforms from small regions around *M* on Fig. 14. Fig. 19 *a* was taken within *M*, and Figs. 19 *b* and *c* were taken at increasing distances above *M*, following the arc of the tubules. The fact that the layer line spot nearest the vertical mask-reflection does not move while the equator rotates about the central maximum shows that the intrarow bridges of one tubule row are sliding past those of the adjacent row. Fig. 19 *c* shows that beyond about 8° of bend arc, the layer line spots shift.

FIGURE 20 A series of transforms from the S.a axostyle shown in Fig. 14, showing the onset of curvature. Fig. 20 *a* corresponds to the region above Fig. 14 where the axostyle is straight. Fig. 20 *b* shows the band of stain precipitate near the top of Fig. 14: already the layer line has begun to broaden. Fig. 20 *c* shows the region below the band of stain precipitate, and the layer line has split into two, although the separation is not as large as is seen further around the curve (Fig. 16).

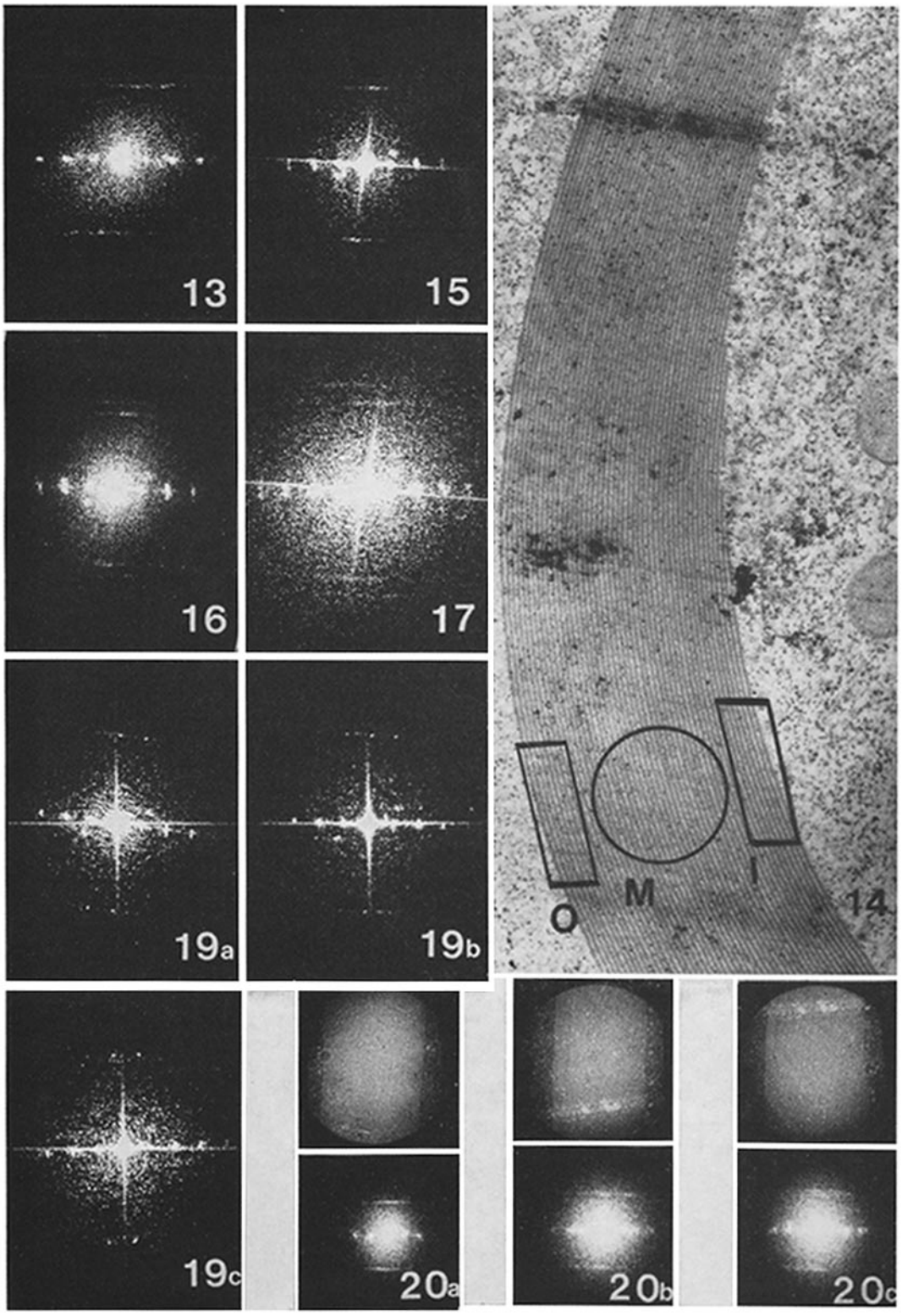
13
15
16
17
19a
19b
19c
20a
20b
20c
O
M
I
14

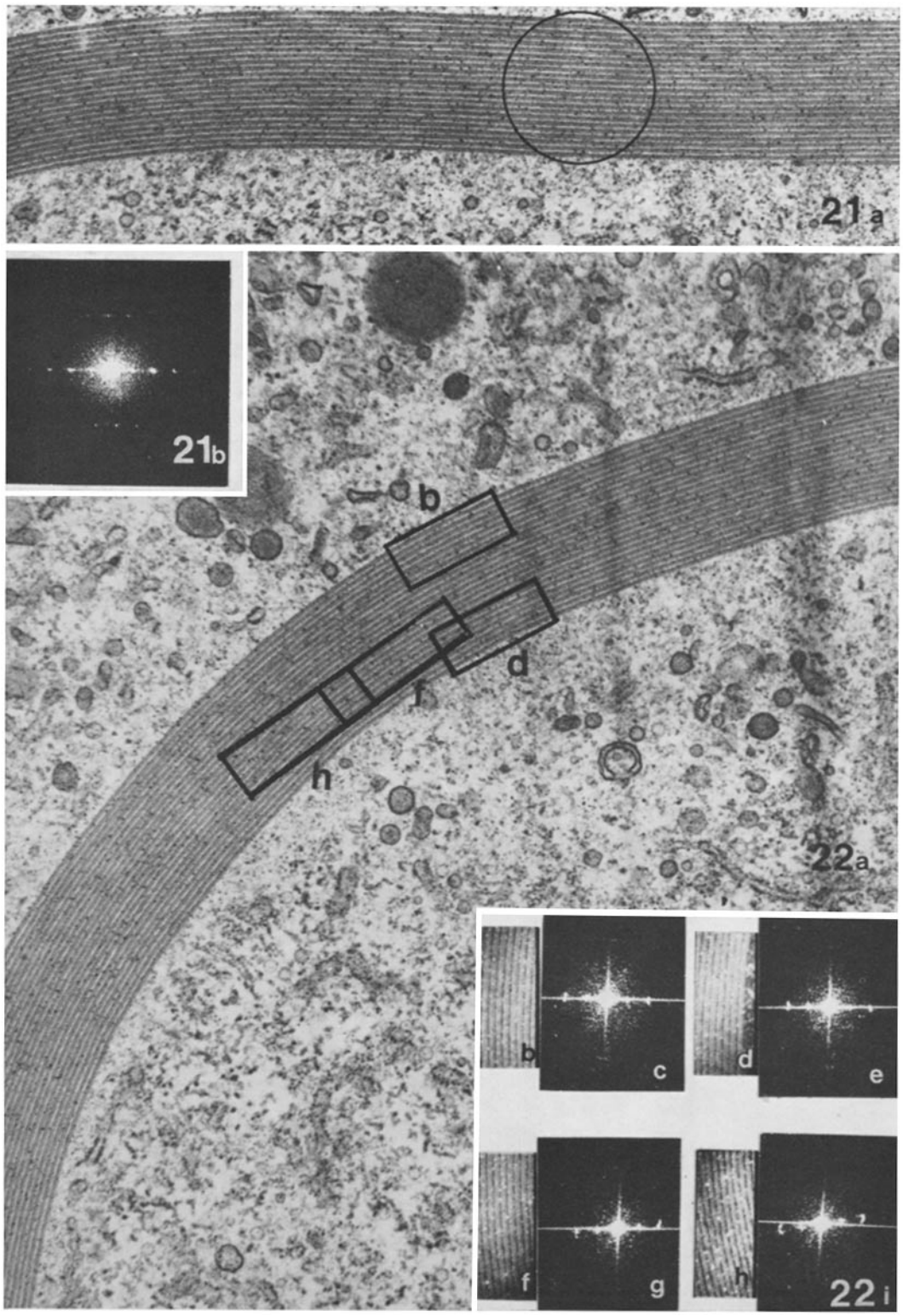

FIGURE 21 S.l axostyle before the onset of curvature. Fig. 21 *a* is continuous with Fig. 22 *a*. The circle on Fig. 21 *a* marks the region transformed in Fig. 21 *b* (21 *b* has been rotated by 90° about an axis perpendicular to the page). A faint layer line is visible at 140 Å. Fig. 21 *a*, × 25,000.

FIGURE 22 Continuation of the S.l curve started in Fig. 21. The rectangles on Fig. 22 *a* show the location of Figs. 22 *b*, *d*, *f*, and *h*. Fig. 22 *c* is the transform of *b*, *e* of *d*, *g* of *f*, and *i* of *h*. A comparison of Figs. 22 *b* and *c* with Figs. 22 *d* and *e* shows that some regions of S.l axostyles show effectively unmeasurable contraction. A comparison of Figs. 22 *f* and *g* with Figs. 22 *h* and *i* shows that in these regions there is limited, direct evidence for sliding. Fig. 22 *a*, × 25,000.

TABLE II

Measurements of Axostyle Contraction in S. lata

Organism	Section	Z	Number of rows
1	1	0.166	23
		0.316	23
		0.266	23
	2	0.006	23
		0.007	23
		0.000	23
	3	0.170	23
		0.197	23
		0.092	23
2	1	0.039	26
	2	0.555	29
		0.594	29
	3	0.208	27
		0.265	27
3	1	0.077	24
		0.075	24
		0.096	24
	2	0.063	24
	3	0.043	29

$$Z = \frac{(P_o - P_i) \text{ observed}}{(P_o - P_i) \text{ theoretical}}.$$

Mean value, $\bar{Z} = 0.167$

$\sigma = 0.169$.

Received for publication 7 April 1972, and in revised form 2 October 1972.

REFERENCES

BANNISTER, L. H., and E. C. TATCHELL. 1968. Contractility and the fiber systems of *Stentor coeruleus*. *J. Cell Sci.* **3**:295.

CLEVELAND, L. R. 1950. Hormone-induced sexual cycles of flagellates. III. Gametogenesis, fertilization, and one-division meiosis in *Saccinobaculus*. *J. Morphol.* **86**:215.

CLEVELAND, L. R., S. R. HALL, E. P. SAUNDERS, and J. COLLIER. 1934. The wood-feeding roach, *Cryptocercus*, its protozoa, and the symbiosis between protozoa and roach. *Mem. Am. Acad. Arts Sci.* **17**:185.

COHEN, C., S. C. HARRISON, and R. E. STEPHENS. 1971. X-ray diffraction from microtubules. *J. Mol. Biol.* **59**:375.

FITZHARRIS, T. P., R. A. BLOODGOOD, and J. R. MCINTOSH. 1972. The effect of fixation on the wave propagation of the protozoan axostyle. *Tissue and Cell.* **4**:219.

GRIMSTONE, A. V., and L. R. CLEVELAND. 1965. The fine structure and function of the contractile axostyle of certain flagellates. *J. Cell Biol.* **25**:387.

HUANG, B. 1970. Ultrastructure of the cortical fiber systems in *Stentor coeruleus* relaxed in ethylene bis (oxyethylene-nitrilo) tetraacetic acid. *J. Cell Biol.* **47** (*2, Pt. 2*):92 a. (Abstr.)

KLUG, A., and J. E. BERGER. 1964. An optical method for the analysis of periodicities in electron micrographs, and some observations on the mechanism of negative staining. *J. Mol. Biol.* **10**:565.

MCINTOSH, J. R., and S. LANDIS. 1971. The distribution of spindle microtubules during mitosis in cultured human cells. *J. Cell Biol.* **49**:468.

MCINTOSH, J. R., E. OGATA, and S. LANDIS. 1973. The axostyle of *Saccinobaculus*. I. Structure of the organism and its microtubule bundle. *J. Cell Biol.* **56**:304.

MCINTOSH, J. R., and K. R. PORTER. 1967. Microtubules in the spermatids of the domestic fowl. *J. Cell Biol.* **35**:153.

SATIR, P. 1965. Studies on cilia. II. Examination of the distal region of the ciliary shaft and the role of the filaments in motility. *J. Cell Biol.* **26**:805.

SUMMERS, K. E., and I. R. GIBBONS. 1971. Adenosine triphosphate-induced sliding of tubules in trypsin-treated flagella of sea-urchin sperm. *Proc. Natl. Acad. Sci. U. S. A.* **68**:3092.

THOMAS, M. B. 1970. Transitions between helical and protofibrillar configurations in doublet microtubules in spermatozoa of *Stylochus zebra*. *Biol. Bull. (Woods Hole).* **138**:219.